Arabian Journal of Chemistry (2020) 13, 6044–6055

King Saud University

Arabian Journal of Chemistry

www.ksu.edu.sa
www.sciencedirect.com

ORIGINAL ARTICLE

Corrosion behavior of AZ91D magnesium alloy in distilled water

Hualiang Huang *, **Wenlu Yang**

School of Chemistry and Environmental Engineering, Key Laboratory of Green Chemical Process of Ministry of Education, Key Laboratory of Novel Reactor and Green Chemical Technology of Hubei Province, Wuhan Institute of Technology, Wuhan 430074, PR China

Received 28 March 2020; accepted 5 May 2020
Available online 19 May 2020

KEYWORDS

AZ91D magnesium alloy;
Distilled water;
Corrosion;
EIS;
SEM

Abstract The corrosion of AZ91D magnesium alloy has received extensive attention due to the continuous expansion of its application field in recent years. However, the corrosion of AZ91D magnesium alloy in distilled water is relatively few. In this paper, the corrosion behavior of AZ91D magnesium alloy was studied in distilled water by electrochemical tests in combination with weight loss and surface analysis methods. The results indicated that the corrosion rate of AZ91D magnesium alloy increased with the increase of temperature and immersion time. The increase of the corrosion rate of AZ91D magnesium alloy with the increase of immersion time might be attributed to the damage of the structure of corrosion product film by hydrogen evolution, significantly accelerating the anodic process of AZ91D magnesium alloy. It was interesting that, in distilled water, the EIS of AZ91D magnesium alloy excluded an inductive arc in the low frequency region, which indicated that there was no the adsorption and desorption of aggressive ions or the damage and repair of film. The corrosion product film of AZ91D magnesium alloy in distilled water was composed of a compact inner corrosion product film and a loose outer corrosion product film.

1. Introduction

China's magnesium resources are abundant, diverse and widely distributed, and the reserves and production of magnesium resources rank first in the world (Shi et al., 2001). Magnesium alloys have many excellent properties, such as lightweight, machinability, shock absorption, dimensional stability and impact resistance (Staiger et al., 2006; Yang et al., 2013; Hänzi et al., 2009; Grosselle et al., 2010; Jiang et al., 1999; Qi et al., 2018). Therefore, magnesium alloys are widely used in a wide range of fields, such as transportation, electronics, medical, military, etc. (Nan and Zheng, 2013; Zhang et al., 2016; Coy et al., 2010; Kwon et al., 2006); and it is increasing gradually. Magnesium alloy die casting is the lightest among all die-casting alloys and a highly competitive automotive lightweight material. A large number of magnesium alloy parts are produced to replace plastic, aluminum alloy and even steel parts (Seetharaman et al., 2017; Abdulov et al., 1990; Wang

* Corresponding author.
E-mail address: 51032265@qq.com (H. Huang).
Peer review under responsibility of King Saud University.

ELSEVIER Production and hosting by Elsevier

https://doi.org/10.1016/j.arabjc.2020.05.004
1878-5352

et al., 2010). Atrens et al. accurately predicted the corrosion rate of Mg alloys in vivo based on laboratory tests (Atrens et al., 2018). Shi et al. evaluated the accuracy of Tafel extrapolation of polarisation curve in determining the corrosion rate of magnesium alloys, and the resulted showed that the corrosion rate could not be estimated by Tafel extrapolation reliably (Shi et al., 2010). Song et al. summarized the various types of magnesium corrosion, which could help people to understand the corrosion processes and how to prevent the corrosion of magnesium alloys (Song and Atrens, 2003). Song et al. also investigated the corrosion mechanism of magnesium alloys and provided the basis for the design of new magnesium alloys (Song and Atrens, 1999). Atrens et al. also introduced the developments in the field of magnesium corrosion (Atrens et al., 2015). With the development of technology and the extension of energy-saving ideas, the application of magnesium alloy in automobile engine can reduce the weight of automobiles, thereby reducing energy consumption and achieving energy savings. However, as the car runs, the engine is heated due to fuel combustion. If the engine is not cooled in time, it will be damaged because of the high temperature (Du and Xu, 2013). Therefore, various coolants are used to reduce engine temperature, such as water, glycol and water mixed liquid.

However, the use of engine coolant is easy to cause the corrosion of magnesium alloy. Magnesium has an equilibrium potential of −2.34 V, so magnesium and magnesium alloys are prone to corrosion, and their corrosion rates are subject to corrosive medium (Cui et al., 2013; Jönsson et al., 2007), alloy compositions (Chen et al., 2019), and other factors (Phani et al., 2015; Song et al., 2004). Qu et al. reported the adsorption and corrosion behavior of trichoderma harzianum for AZ31B magnesium alloy in artificial seawater (Qu et al., 2017), and the experimental results showed that the fungus reduced the corrosion of metals. Liao et al. reported the atmospheric corrosion behavior of field-exposed magnesium alloys (Liao and Hotta, 2015), and their research results showed that the corrosion resistance of magnesium alloys generally increased with the increase of Al content, and the corrosion in the marine environment was more serious than the urban environment. Li et al. reported that effect of rare-earth element samarium (Sm) on the corrosion behavior of Mg6Al1.2Y-0.9Nd alloy, and the results showed that, with the increasing Sm content, the corrosion rate of the alloy decreased at first, then increased and reached the valley at 0.5 wt% Sm. The addition of Sm element made the microstructure of the alloy uniform and significantly improved the corrosion resistance of the alloy (Li et al., 2010).

The corrosion behavior of magnesium alloy in engine coolant, such as glycol solution, sodium sulfate solution and sodium chloride solution, has been studied. Huang et al. (Huang et al., 2012) studied the corrosion behavior of magnesium alloy in ethylene glycol water solution by electrochemical methods, and the results indicated that the corrosion rate of AZ91D magnesium alloy decreased with increasing concentration of ethylene glycol. Medhashree et al. (Medhashree and Shetty, 2017) reported that corrosion behavior of magnesium alloys in solutions containing different concentrations of sulfate ions, and the results showed that the corrosion rate increased with the increase of sulfate ion concentration and temperature, and decreased with increasing pH. In addition, Arrabal et al. (Arrabal et al., 2012) studied the corrosion of magnesium alloy in 3.5% NaCl solution, and the results showed that the corrosion of magnesium alloy was very serious in 3.5% NaCl solution, and the addition of neodymium (Nd) element could delay the corrosion. In fact, due to the poor corrosion resistance of magnesium alloy, the water solution containing chloride ions is not generally used as automobile engine coolant, especially sea water. In winter, in order to prevent water from freezing at a low temperature, glycol is usually added to water to reduce the freezing point of water. Some studies have shown that when the mixture of glycol and water is used as engine coolant, the corrosion of magnesium alloy is main related to water, but not glycol (Huang et al., 2012). Moreover, glycol plays a certain role in inhibiting the corrosion of magnesium alloy. Therefore, it is very important to study the corrosion mechanism of magnesium alloy in distilled water.

AZ91D magnesium alloy has the characteristics of high specific strength and corrosion resistance. Therefore, it can be used to construct automobile engine. However, the corrosion behavior and mechanism of AZ91D magnesium alloy are not investigated in distilled water. Although the conductivity of distilled water is very low, or almost non-conductive, the formation of magnesium ions and hydroxide ions can increase the conductivity of water after magnesium reacts with water due to the high activity of magnesium (Cui et al., 2013; Jönsson et al., 2007), which further accelerates the corrosion of magnesium alloy.

In this paper, the corrosion behavior and mechanism of AZ91D magnesium alloy in distilled water were studied by weightlessness, electrochemical measurements and surface analysis technologies, the effects of temperature and immersion time on the corrosion of AZ91D magnesium alloy were clarified, and the corrosion dynamic behavior of AZ91D magnesium alloy in distilled water was also studied. This study provides the basic theoretical basis for the corrosion protection of automobile engine in coolant.

2. Experimental

2.1. Materials and solutions

The AZ91D magnesium alloy was selected because of good machinability and lightweight in this experiment, and its chemical compositions were Al (9%), Zn (1%), Mn (0.3%) and Mg (balance). A cylindrical specimen processed from AZ91D magnesium alloy sample was used for electrochemical tests. A small hole was drilled at one end of the specimen, and then a copper wire passed through the hole and was screwed firmly, and then the gap between the copper wire and the specimen was filled with solder to strengthen the electrical connection between magnesium alloy and copper wire, ensuring electrochemical tests. Finally, the specimen was encapsulated by epoxy resin, leaving only the other end of the specimen as a working surface (0.95 cm^2). Before electrochemical tests, the working surface of the specimen was first sanded with different mesh grit silicon carbide papers (600#, 800#, 1000#) from small to large, and then polished by using metallographic sandpaper. Finally, the surface polished was rinsed with distilled water and absolute ethanol, and then placed it in vacuum drying oven for spare. The solution used in this experiment was distilled water. The test temperatures were 30 °C, 40 °C, and 50 °C, respectively.

2.2. Weightlessness tests

The AZ91D magnesium alloy sample was machined into cuboid specimen with the size of 50 mm × 10 mm × 2 mm, and the pretreatment method of the specimen is the same as that of the electrochemical test specimen. The initial quality (M_0) was weighed using an electronic balance (accuracy is 0.1 mg). The specimen was immersed in distilled water at different temperatures of 30 °C, 40 °C, and 50 °C for 24 h. After immersion test, the corroded specimens were taken out from distilled water, washed with deionized water and dried, and then immersed again in pickling solution (Cr_2O_3 200 g/L + $AgNO_3$ 10 g/L) for 5–10 min to remove surface corrosion products. Finally, the specimens removed corrosion products were washed by deionized water and dried, and weighed using the electronic balance again (M_1). Therefore, the weightlessness (ΔM) could be calculated. For weightlessness tests, three groups of parallel specimens were used to obtain the average corrosion weightlessness.

2.3. Electrochemical tests

The potentiodynamic polarization curve and electrochemical impedance spectroscopy (EIS) measurements were carried out using a CS350 electrochemical measurement system, adopting traditional three-electrode system, in which a saturated calomel electrode (SCE) placed on a glass salt bridge filled with saturated potassium chloride agar was used as reference electrode (RE) and a platinum electrode was used as counter electrode (CE). A specimen prepared was used as working electrode (WE). After the open circuit potential (OCP) of the specimen reached a stable state, the EIS was measured at an amplitude of 10 mV over the OCP over a scan frequency range of 10^{-2} Hz to 10^5 Hz. And then the polarization curve measurement was performed, the scanning rate was 1.0 mV/s, and the scanning potential range was from −500 mV (SCE) to + 500 mV (SCE). All electrochemical tests were repeated at least three times.

2.4. Characterization of surface morphologies and corrosion products

After corrosion for 24 h, the surface and cross-sectional morphologies of the corroded specimens were observed by scanning electron microscopy (SEM). The composition of corrosion products was analyzed by X-ray photoelectron spectroscopy (XPS) and X-ray diffraction (XRD).

3. Results and discussion

3.1. OCP measurements

Fig. 1 shows the time dependence of the corrosion potentials of AZ91D magnesium alloy with different temperatures in distilled water. It is seen from Fig. 1 that, as temperature increases, the corrosion potentials of AZ91D magnesium alloy negatively shift, indicating the significant acceleration of its anodic process. Meanwhile, the corrosion potentials of AZ91D magnesium alloy increase gradually with the increase of immersion time and then reach a stable state, which can be attributed to the inhibition of its anodic process due to the gradual formation of corrosion products with the increase of immersion time at the beginning of corrosion. In the later stage of corrosion, the cathode and anode processes are relatively stable, resulting in relatively stable corrosion potentials.

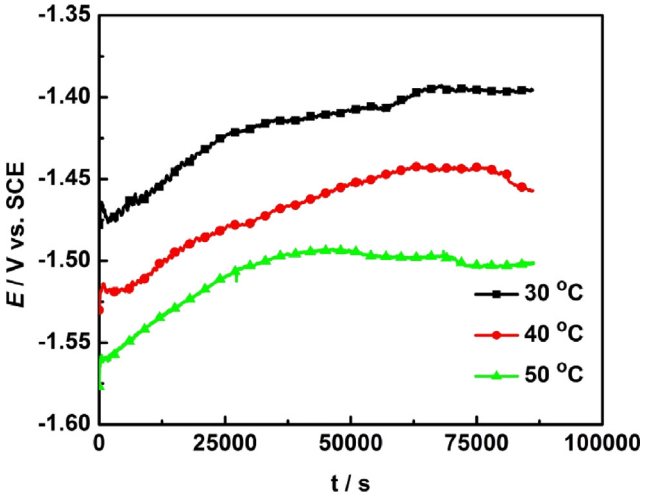

Fig. 1 The time dependence of the OCP of AZ91D magnesium alloy in distilled water at 30 °C, 40 °C and 50 °C for 24 h.

3.2 Weight. loss measurements

The results of the weight loss measurements are more directly and accurately characterize the corrosion rate of metals than others, such as corrosion current density, corrosion resistance. The formula for calculating corrosion rate using the weight loss method (Raj and Rajendran, 2013; Aljinović et al., 2000) is as follows:

$$v = \frac{M_0 - M_1}{S \times t} \quad (1)$$

Here, v represents corrosion rate, M 0 is the quality of metal before corrosion, M 1 is the quality of metal without corrosion products after corrosion, S is the corrosion area of specimen, t is the corrosion time of specimen.

Table 1 lists the corrosion rates of AZ91D magnesium alloy after soaking for 24 h and 96 h at different temperatures. It is seen from Table 1 that, as temperature and immersion time increase, the corrosion rates of AZ91D magnesium alloy increase.

Table 1 The corrosion rates of AZ91D magnesium alloy with different immersion time in distilled water at 30 °C, 40 °C and 50 °C.

Time (h)	T (°C)	v (mg·cm^{-2}·d^{-1})
24	30	4.75
	40	5.19
	50	6.38
96	30	5.91
	40	6.72
	50	8.44

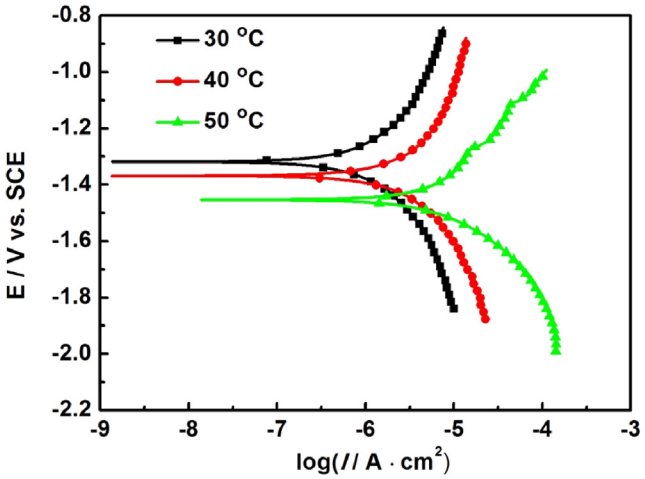

Fig. 2 Polarization curves ofAZ91D magnesium alloy in distilled water at 30 °C, 40 °C and 50 °C for 24 h.

3.3. Polarization curve tests

Fig. 2 presents the polarization curves of AZ91D magnesium alloy after soaking for 24 h at 30 °C, 40 °C, and 50 °C, respectively. It is seen from Fig. 2 that, as temperature increases, the cathodic and anodic current densities increase. This indicates that the corrosion rates of AZ91D magnesium alloy increase with the increase of temperature. Moreover, the self-corrosion potentials shift negatively, which indicates that the acceleration of the anode process of AZ91D magnesium alloy is more significant than that of its cathode process with the increase of temperature. This may be attributed to the damage of corrosion product film caused by hydrogen evolution, which accelerates the anodic dissolution of magnesium alloy. Based on the corrosion mechanism of magnesium alloys in neutral aqueous solution (Song et al., 1997), the anode process is the dissolution of magnesium, and the cathode process is the hydrogen evolution of water. Therefore, the precipitation of hydrogen leads to the damage of corrosion product film.

Generally, the corrosion current density can be obtained by the Tafel extrapolation of potentiodynamic polarization curve. Considering the influence of the formation and rupture of the surface film on the anodic process, the cathode Tafel extrapolation is used to fit the polarization curve of AZ91D magnesium alloy in this paper, and the corresponding fitting results of corrosion potential (E_{corr}), corrosion current density (I_{corr}), and cathodic Tafel slopes (b_c) in these polarization curves are listed in Table 2.

E_{corr} and I_{corr} are two very significant physical quantities for judging the difficulty of metal corrosion. Usually, the more negative the E_{corr} is, the higher the activity of the electrode is, and the more likely the electrode is to corrode. It is generally known that I_{corr} nearly directly characterizes the corrosion rate of metal at E_{corr}, and the larger the I_{corr} is, the faster the corrosion rate of metal is (Arrabal et al., 2012). It is seen from Table 2 that the E_{corr} negatively shifts from −1.32 V (SCE) to −1.45 V (SCE) with the increase of temperature, which indicates that the increase of temperature may increase the activity of the electrode and accelerate the corrosion of AZ91D magnesium alloy. Meanwhile, as temperature increases, the I_{corr} increases from 6.64×10^{-7} A·cm^{-2} to 4.56×10^{-6} A·cm^{-2}, which indicates that the increase of temperature significantly promotes the anode process of AZ91D magnesium alloy, resulting in the acceleration of the corrosion of AZ91D magnesium alloy. In order to compare numerically with the corrosion rate obtained by weightlessness, the corrosion rate (mm/y) is calculated by the I_{corr} and listed in Table 2. It is seen from Table 2 that the results of polarization curve tests are consistent with that of weightlessness tests.

3.4. EIS measurements

In order to further understand the corrosion mechanism of AZ91D magnesium alloy in distilled water, we measured the EIS of AZ91D magnesium alloy in distilled water at different temperatures and different time. Fig. 3 shows the EIS of AZ91D magnesium alloy in distilled water at different temperatures for 24 h. Interestingly, it can be seen from Fig. 3a that there are three capacitive arcs, rather than the two arcs previously reported (Arrabal et al., 2012). It can be also seen from Fig. 3b that there are three time constants. This indicates that each capacitive arc corresponds to a time constant. The capacitive arc in the high frequency region may represent a capacitive response of inner corrosion product film on the electrode surface, the capacitive arc in the intermediate frequency region represents a capacitive response of outer corrosion product film, and the capacitive arc in the low frequency region represents a charge transfer process (Fekry and El-Sherif, 2009). It is worth noting that; in this study, there is no inductive arc in the low frequency region, which indicates that there is no unsteady process on the electrode surface, such as the adsorption and desorption of ions/inhibitors (Zhang et al., 2011); the damage and repair of film (Song et al., 2008). This may be because the distilled water does not contain chloride ions and inhibitors, and the oxide film or corrosion product film on the metal surface is not repaired.

Furthermore, as temperature increases, the diameter of each capacitive loop is gradually reduced. Moreover, it can be seen from Fig. 3b that the modulus of impedance also decreases with the increase of temperature. This indicates that, with the increase of temperature, the resistances of corrosion product films and charge transfer resistance decrease gradually, resulting in the increase of the corrosion rate of AZ91D

Table 2 The fitting parameters of the polarization curves of AZ91D magnesium alloy in distilled water at 30 °C, 40 °C and 50 °C for 24 h.

T (°C)	B_c (mV/dec)	I_{corr} (A/cm^2)	E_{corr} (V)	corrosion rate (mm/y)
30	−239.59	6.64×10^{-7}	−1.319	0.0146
40	−202.73	1.29×10^{-6}	−1.369	0.0284
50	−182.99	4.56×10^{-6}	−1.455	0.1003

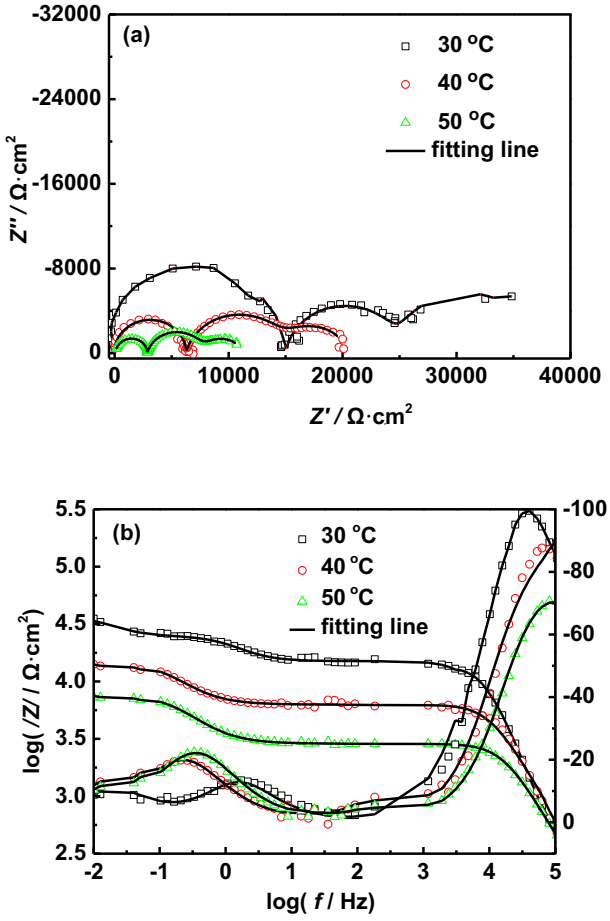

Fig. 3 EIS ofAZ91D magnesium alloy in distilled water at 30 °C, 40 °C and 50 °C for 24 h: (a) Nyquist plots, (b) Bode plots.

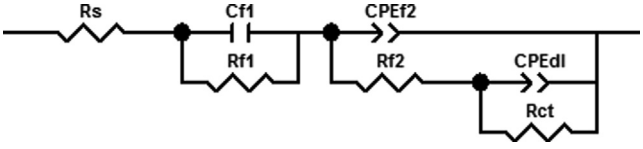

Fig. 4 The equivalent circuit used for fitting the EIS data of AZ91D magnesium alloy in distilled water.

magnesium alloy. The decrease of the resistance of corrosion product film may be explained as follows: the increase of temperature accelerates the corrosion of AZ91D magnesium alloy, which leads to the production of more hydrogen caused by the cathode reaction, eventually resulting in a more loose corrosion product film.

Based on the above analysis, the equivalent circuit shown in Fig. 4 is used to fit the EIS data to obtain the corresponding

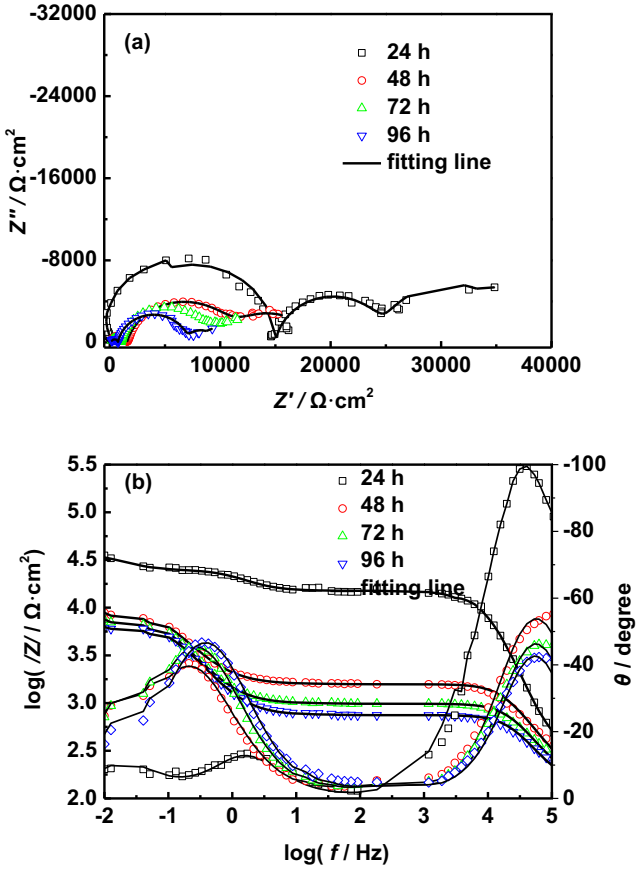

Fig. 5 EIS of AZ91D magnesium alloy with different immersion time in distilled water at 30 °C: (a) Nyquist plots, (b) Bode plots.

impedance parameters, and the corresponding values of these impedance parameters are listed in Table 3. Where, R_s represents a solution resistance, C_{f1} represents a capacitance response of inner corrosion product film, R_{f1} represents a film resistance of the inner corrosion product film, CPE_{f2} represents a capacitance response of outer corrosion product film, n_{f2} represents the index of the dispersion effect related to the outer corrosion product film, R_{f2} represents a film resistance of the outer corrosion product film, CPE_{dl} represents a double layer capacitance, n_{dl} represents the index of the dispersion effect related to the double layer between electrode and solution, R_{ct} represents a charge transfer resistance of corrosion electrochemical reaction.

It can be seen from Table 3 that the R_{ct} decreases with the increase of temperature, which indicates that the increase of temperature accelerates the corrosion of AZ91D magnesium alloy. Moreover, the R_{f1} and R_{f2} also decrease with the increase of temperature, which can be attributed that hydrogen evolution in cathode process damages the structure of

Table 3 The EIS fitting results of AZ91D magnesium alloy in distilled water at 30 °C, 40 °C and 50 °C for 24 h.

T (°C)	R_s (Ω·cm²)	C_{f1} (F·cm^{-2})	R_{f1} (Ω·cm²)	CPE_{f2} (S·s^{nf1}·cm^{-2})	n_{f2}	R_{f2} (Ω·cm²)	CPE_{dl} (S·s^{nf2}·cm^{-2})	n_{dl}	R_{ct} (Ω·cm²)
30	126.70	2.19×10^{-9}	15,139	1.55×10^{-5}	0.93	10,258	6.87×10^{-4}	0.92	12,020
40	52.36	2.45×10^{-9}	6315	1.13×10^{-5}	0.86	9031	4.54×10^{-4}	0.83	5241
50	85.06	3.50×10^{-9}	2769	1.53×10^{-5}	0.85	5042	9.38×10^{-4}	0.77	3431

corrosion product film, resulting that corrosion product film becomes looser. Furthermore, the higher temperature is, the faster the corrosion rate of AZ91D magnesium alloy is, the more hydrogen release, and the more serious the damage of corrosion product film is.

In order to further investigate the effect of immersion time on the corrosion of AZ91D magnesium alloy in distilled water, Figs. 5–7 shows the EIS of AZ91D magnesium alloy in distilled water at different temperatures for 96 h. Interestingly, it can be seen from Figs. 5 and 6 that the diameters of all capacitive arcs decrease with the increase of immersion time at 30 °C and 40 °C, especially the capacitive arc in the high frequency region, which indicates that the total corrosion impedance of AZ91D magnesium alloy decreases gradually with the increase of immersion time at 30 °C and 40 °C. Therefore, the corrosion rate of AZ91D magnesium alloy increases gradually with the increase of immersion time at 30 °C and 40 °C, which can be explained as follows: with the prolongation of immersion time, hydrogen evolution caused by corrosion electrochemical reaction damages the structures of corrosion product films and makes the corrosion product films more loose, which reduces the protection of corrosion product films, and finally accelerates the corrosion of AZ91D magnesium alloy. The reduction of the diameters of the capacitive arcs corresponding to corrosion product films confirms these results.

At 50 °C, it can be seen from Fig. 7 that the diameter of the capacitive arc in the high frequency region rapidly decreases after 48 h immersion, which can be attributed that hydrogen evolution caused by corrosion electrochemical reaction damages the structures of corrosion product films. However, the diameters of the capacitive arcs in the intermediate and low frequency region have no obvious change, which demonstrates that the total corrosion impedance of AZ91D magnesium alloy first decreases and then remains relatively stable. This can be explained as follows: with the further increase of temperature, the corrosion of AZ91D magnesium alloy is intensified, which results in a large number of hydrogen precipitation, seriously damaging the structure of corrosion product film at the beginning of corrosion. In the later stage of corrosion, although the corrosion products are further formed and accumulated, the impedance of the corrosion product film has no significant change due to the damage of the structure of corrosion product film caused by hydrogen evolution. Therefore, the impedance of corrosion electrochemical reaction remains relatively stable.

To further confirm the above analysis, the EIS of AZ91D magnesium alloy in distilled water at different temperatures for 96 h is fitted by using the equivalent circuit shown in Fig. 4, and the corresponding values of these impedance

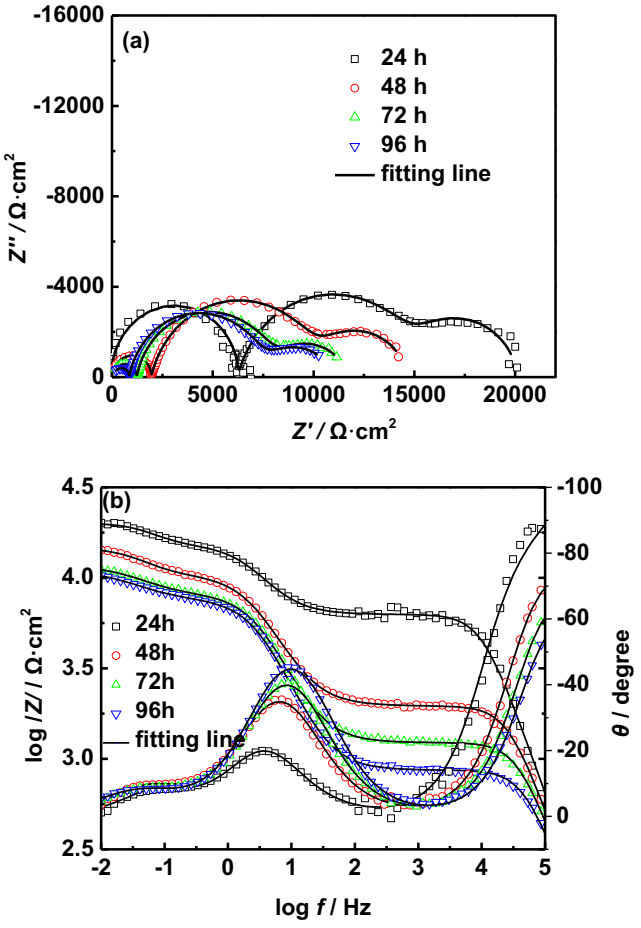

Fig. 6 EIS of AZ91D magnesium alloy with different immersion time in distilled water at 40 °C: (a) Nyquist plots, (b) Bode plots.

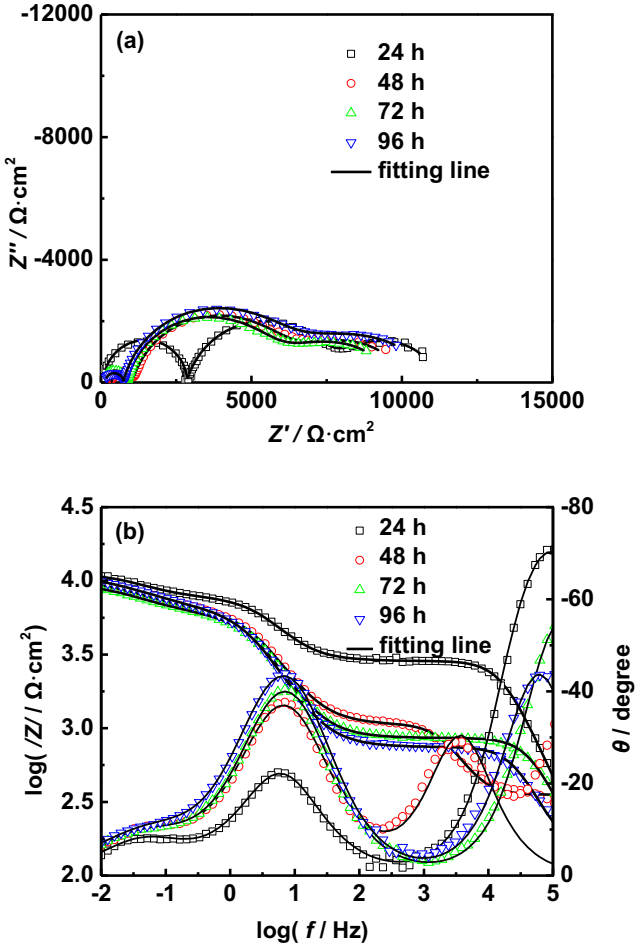

Fig. 7 EIS of AZ91D magnesium alloy with different immersion time in distilled water at 50 °C: (a) Nyquist plots, (b) Bode plots.

Table 4 The EIS fitting results of AZ91D magnesium alloy with different immersion time in distilled water at 30 °C.

Time (h)	R_s (Ω·cm^2)	C_{f1} (F·cm^{-2})	R_{f1} (Ω·cm^2)	CPE_{f2} (S·s^{nf1}·cm^{-2})	n_{f2}	R_{f2} (Ω·cm^2)	CPE_{dl} (S·s^{nf2}·cm^{-2})	n_{dl}	R_{ct} (Ω·cm^2)
24	126.70	2.19×10^{-9}	15,139	1.55×10^{-5}	0.93	10,258	6.87×10^{-4}	0.92	12,020
48	167.7	6.11×10^{-8}	1401	2.01×10^{-5}	0.84	9978	8.70×10^{-4}	0.77	6980
72	157.5	8.63×10^{-9}	821.1	1.99×10^{-5}	0.87	8350	1.09×10^{-3}	0.81	4858
96	143.4	1.12×10^{-8}	600.2	1.81×10^{-5}	0.89	6412	3.63×10^{-3}	0.93	2414

Table 5 The EIS fitting results of AZ91D magnesium alloy with different immersion time in distilled water at 40 °C.

Time (h)	R_s (Ω·cm^2)	C_{f1} (F·cm^{-2})	R_{f1} (Ω·cm^2)	CPE_{f2} (S·s^{nf1}·cm^{-2})	n_{f2}	R_{f2} (Ω·cm^2)	CPE_{dl} (S·s^{nf2}·cm^{-2})	n_{dl}	R_{ct} (Ω·cm^2)
24	52.36	2.45×10^{-9}	6315	1.12×10^{-5}	0.86	9031	4.54×10^{-4}	0.83	5241
48	48.30	3.06×10^{-9}	1905	1.16×10^{-5}	0.85	8541	7.50×10^{-4}	0.86	4200
72	67.92	3.52×10^{-9}	1158	1.15×10^{-5}	0.87	6994	9.32×10^{-4}	0.79	3501
96	72.68	4.11×10^{-9}	790.4	1.16×10^{-5}	0.88	6800	1.09×10^{-3}	0.76	3331

Table 6 The EIS fitting results of AZ91D magnesium alloy with different immersion time in distilled water at 50 °C.

Time (h)	R_s (Ω·cm^2)	C_{f1} (F·cm^{-2})	R_{f1} (Ω·cm^2)	CPE_{f2} (S·s^{nf1}·cm^{-2})	n_{f2}	R_{f2} (Ω·cm^2)	CPE_{dl} (S·s^{nf2}·cm^{-2})	n_{dl}	R_{ct} (Ω·cm^2)
24	85.06	3.50×10^{-9}	2769.0	1.53×10^{-5}	0.85	5042	9.38×10^{-4}	0.77	3431
48	354.00	1.06×10^{-7}	696.2	1.92×10^{-5}	0.84	5462	8.30×10^{-4}	0.69	3758
72	81.11	4.51×10^{-9}	775.6	1.94×10^{-5}	0.86	5188	8.26×10^{-4}	0.68	3804
96	136.5	$9.99 \times 10^{-}$	606.9	2.03×10^{-5}	0.86	5842	6.44×10^{-4}	0.64	4567

parameters are listed in Tables 4–6. It is seen from Tables 4 and 5 that the R_{f1}, R_{f2} and R_{ct} decrease with the prolongation of immersion time, which is attributed to the damage of the structure of corrosion product film caused due to hydrogen evolution. The decrease of the R_{ct} indicates the increase of the corrosion rate of AZ91D magnesium alloy. It is seen from Table 6 that the R_{f1} first decreases rapidly and then remains relatively stable with the prolongation of immersion time, and the R_{f2} and R_{ct} remain relatively stable with the prolongation of immersion time. By comparing the R_{f1} and R_{f2} at different temperatures, we find that the R_{f1} and R_{f2} are the smallest at 50 °C, which can be attributed to more severe corrosion of AZ91D magnesium alloy, resulting in more serious damage of the structure of corrosion product film caused due to hydrogen evolution. Generally, the corrosion rates of metals can be characterized by the reciprocal of polarization resistance (R_p). In this paper, the R_p is equal to the sum of R_{f1}, R_{f2} and R_{ct} ($R_p = R_{f1} + R_{f2} + R_{ct}$). Fig. 8 presents the R_p of AZ91D magnesium alloy at different temperature and soaking time. It is seen from Fig. 8 that the R_p decreases with the increase of temperature and immersion time in the early stages of corrosion, which indicates the corrosion rate of AZ91D magnesium alloy increases with the increase of temperature and immersion time. In the last stage of corrosion, the corrosion rate of AZ91D magnesium alloy tends to be relatively stable.

3.5. SEM surface morphologies

Fig. 9 is the surface micro-morphologies of AZ91D magnesium alloy immersed in distilled water for 24 h at different temperatures. It can be seen from Fig. 9 that AZ91D magnesium alloy has different degrees of corrosion at different temperatures, and its corrosion becomes more serious with the increase of temperature. At 30 °C, there are a few loose corrosion products and small blowholes caused by hydrogen evolution on the surface of AZ91D magnesium alloy. Compared with 30 °C, the corrosion products and blowholes on the surface of AZ91D magnesium alloy increase at 40 °C, and the corrosion products is more loose. At 50 °C, there are many sheet corrosion products and some cracks on the surface of AZ91D magnesium

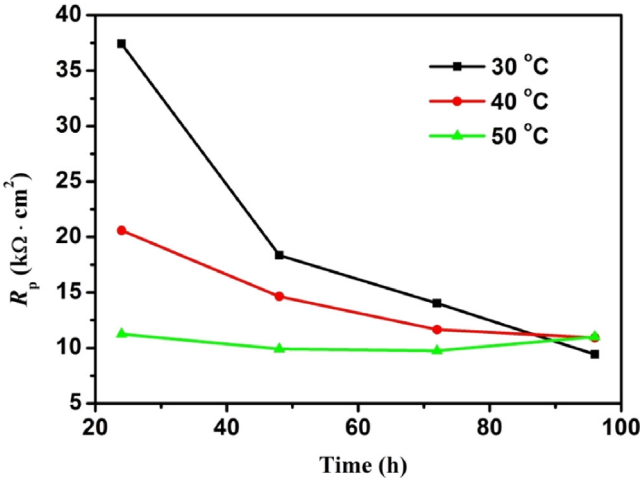

Fig. 8 The polarization resistance of AZ91D magnesium alloy at different temperature and soaking time.

alloy, which indicates that AZ91D magnesium alloy is seriously corroded. However, there is no blowhole on the surface of AZ91D magnesium alloy, which may be due to the intensified corrosion of AZ91D magnesium alloy at 50 °C, leading to a large amount of hydrogen evolution and seriously damaging the structure of corrosion product film, eventually resulting that the corrosion products is more loose. Comparing the surface micro-morphologies of AZ91D magnesium alloy at different temperatures, we find that, at 50 °C, the more the corrosion products, the looser the corrosion products, and the more serious the corrosion of AZ91D magnesium alloy.

Fig. 10 presents the cross-sectional scan morphologies with different locations of AZ91D magnesium alloy after soaking in distilled water at 30 °C for 24 h. It can be observed from Fig. 10a that the corrosion product film consists of two layers, i.e. the compact inner layer and the relatively loose outer layer. This is consistent with the result of impedance tests. It can be observed from Fig. 10 that the corrosion product film is relatively complete in some places, the corrosion product film begins to crack in some places, the corrosion product film has already been broken in some places, and the corrosion products have fallen off in some places. This may be due to the dissolution of AZ91D magnesium alloy α phase, accompanying hydrogen evolution, resulting in the damage of corrosion product structure. This is consistent with that of the EIS tests.

3.6. The composition of corrosion products

Fig. 11 shows the XRD spectrum of AZ91D magnesium alloy after immersion in distilled water at 30 °C for immersion 24 h. It can be observed that magnesium oxide, magnesium hydroxide, and magnesium aluminum oxyhydrogen compound (including magnesium hydroxide and aluminum hydroxide) are present in corrosion products (Zhang and Zuo, 2019; Lu et al., 2015).

In order to further confirm the composition of the surface film of AZ91D magnesium alloy, Fig. 12 shows the XPS measurement spectrum and high score spectrum spectra of AZ91D

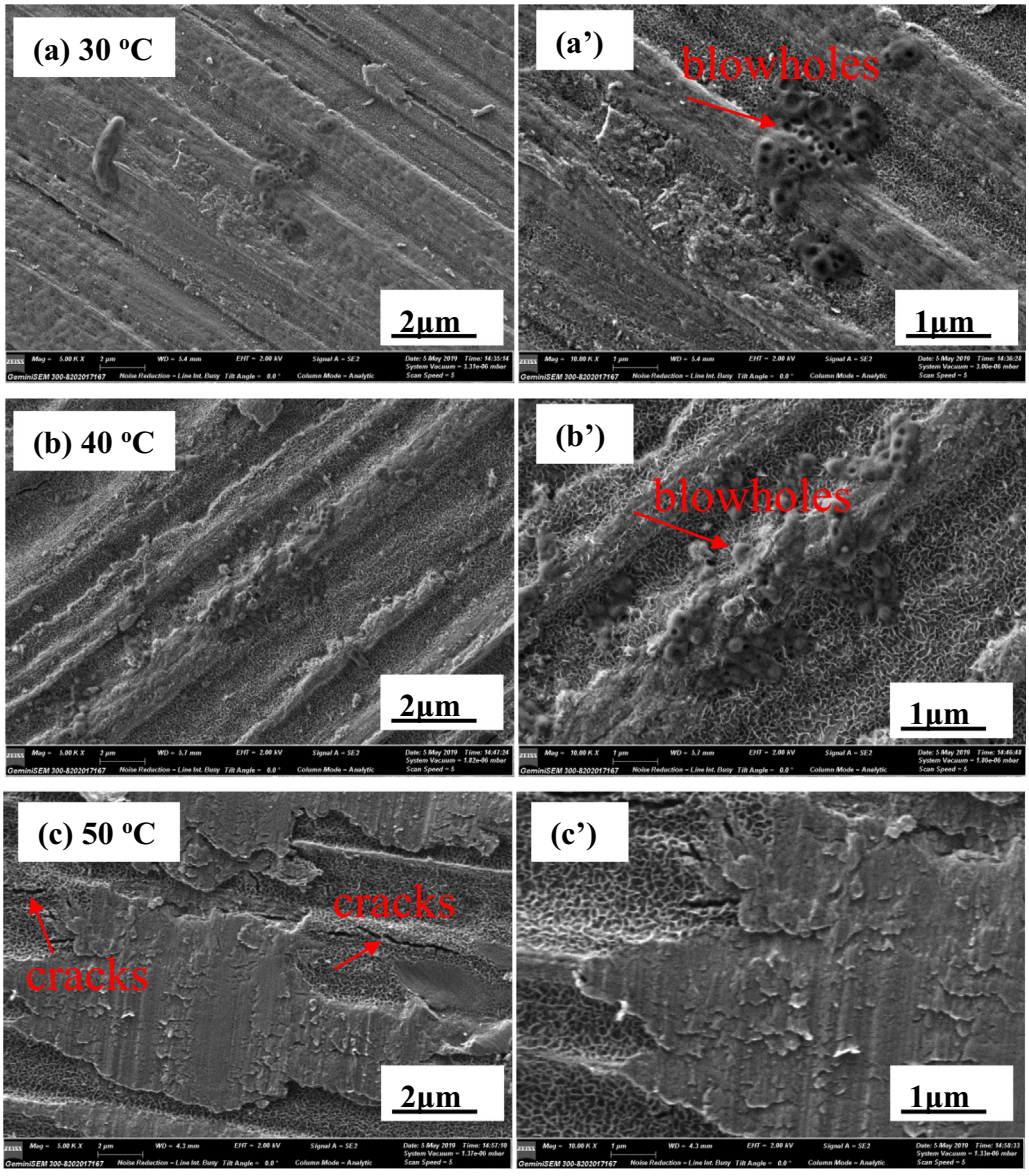

Fig. 9 SEM surface morphologies of AZ91D magnesium alloy in distilled water at 30 °C, 40 °C and 50 °C for 24 h.

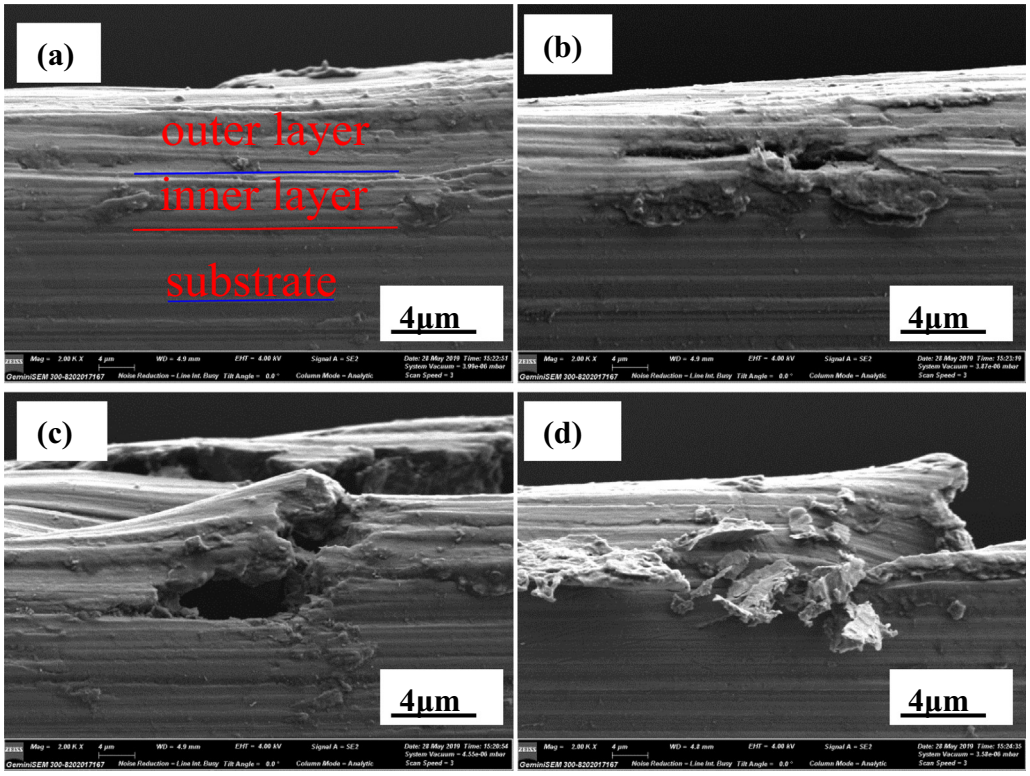

Fig. 10 The cross-sectional morphologies of AZ91D magnesium after soaking in distilled water for 24 h at 30 °C.

magnesium alloy in distilled water solution at 30 °C for soaking 24 h. It is observed from Fig. 12a that the peaks of Mg 1 s, O 1 s and Al 2p are detected on the AZ91D magnesium alloy surface. This is consistent with the results of XRD analysis results. Fig. 12b shows the high resolution peaks of O 1 s. The O 1 s spectrum is composed of three peaks. The peak at 530.9 eV can originate from O^{2-}, related to the presence of MgO. The peaks at 531.5 eV and 532.1 eV can be ascribed to OH^{-}, related to the presence of $Mg(OH)_2$ and $Al(OH)_3$ (Mehta et al., 2004). The Al 2p spectrum is composed of just one peak. The peak at 74.2 eV can be stemmed from Al $(OH)_3$, related to the presence of magnesium aluminum oxyhydrogen compound.

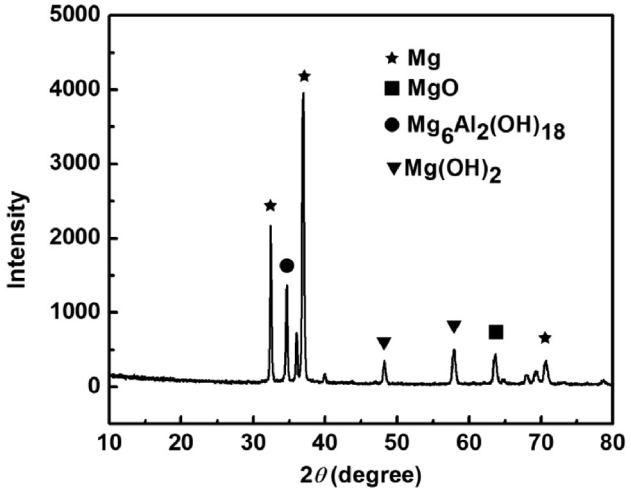

Fig. 11 XRD of the surface film of AZ91D magnesium alloy in distilled water at 30 °C for 24 h immersion.

3.7. The activation energy of AZ91D magnesium alloy in distilled water

Generally, the activation energy (E_a) represents the resistance of a reaction, and the higher the activation energy is, the more difficult the reaction is. In order to determine the effect of immersion time on the corrosion rate of AZ91D magnesium alloy in distilled water, the E_a of the corrosion reactions of AZ91D magnesium alloy in distilled water can be determined according to the Arrhenius equation as follows (Zhang et al., 2019):

$$\ln I_{corr} = -\frac{E_a}{R}\frac{1}{T} + \ln A \quad (2)$$

where, A is the Arrhenius pre-exponential factor, R is the gas constant, the *I*corr of AZ91D magnesium alloy at different immersion time is determined by polarization curve measurements in distilled water. In this paper, we use the reciprocal of *R*p instead of the *I*corr to obtain the *E*a of AZ91D magnesium alloy at different immersion time.

Fig. 13 shows the plots of ln(1/*R*p) vs. 1/*T* of AZ91D magnesium alloy in distilled water. The *E*a can be obtained by the slope (-*E*a/R) of the line, and the value is listed in Table 7. It is seen from Table 7 that, with the increase of immersion time, the *E*a decreases from 49.99 kJ/mol to −6.48 kJ/mol, which indicates the corrosion reactions are easier as the immersion time increases. This may be explained as follows: with the increase of immersion time, more hydrogen caused by cathode

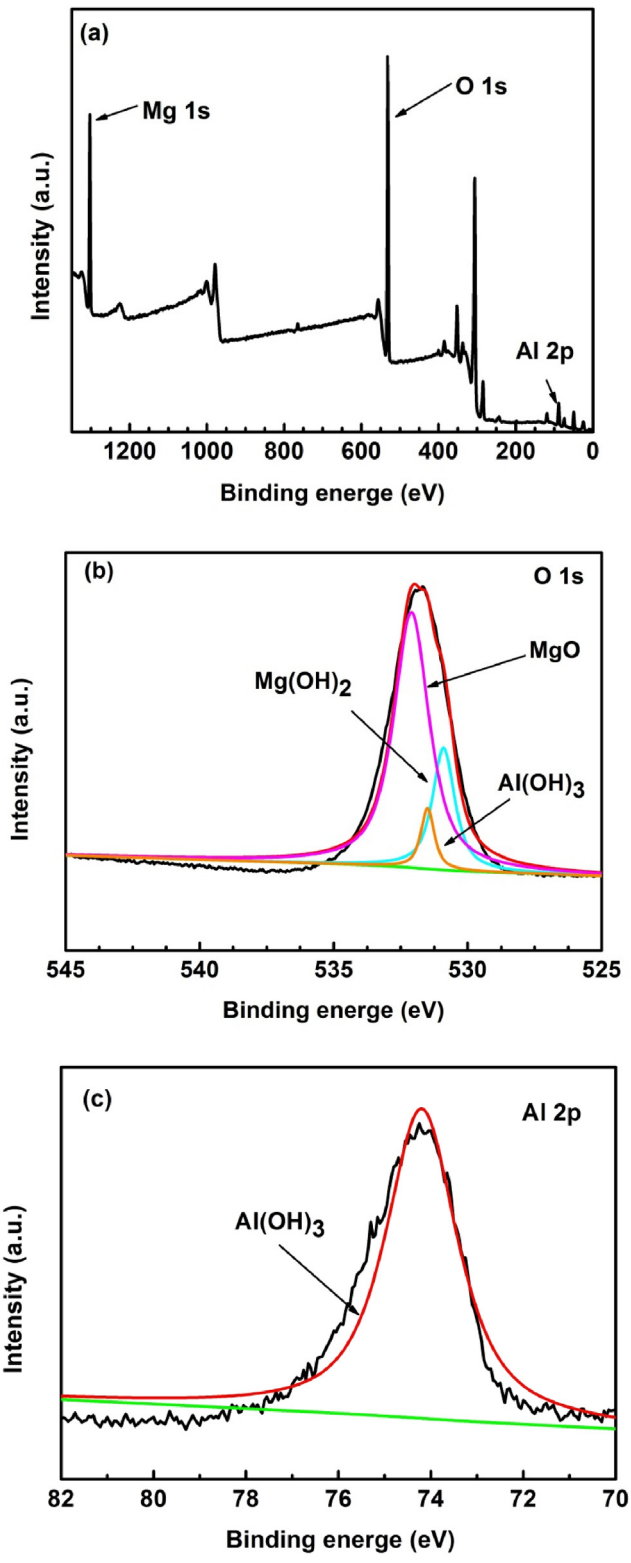

Fig. 12 XPS of the surface film of AZ91D magnesium alloy in distilled water at 30 °C for 24 h immersion: (a) survey spectra, (b) O 1 s, (c) Al 2p.

process release, which seriously damages the structure of corrosion product film and leads to more loose corrosion product film, eventually reducing the resistance of corrosion reactions.

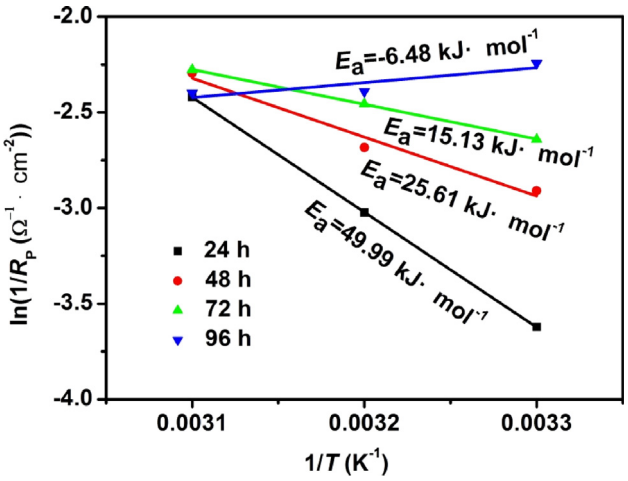

Fig. 13 The plots of ln(1/*R*p) vs. 1/*T* of AZ91D magnesium alloy at different immersion time in distilled water.

Table 7 The E_a of AZ91D magnesium alloy at different immersion time in distilled water.

Time (h)	E_a (kJ/mol)	Linear correlation coefficient
24	49.99	0.999
48	25.61	0.977
72	15.13	0.999
96	−6.48	0.791

4. Conclusions

In this paper, the corrosion behavior of AZ91D magnesium alloy has been investigated in distilled water by weight loss, electrochemical measurements and surface analysis technologies. The results are as follows:

1. With the increase of temperature, the corrosion potentials of AZ91D magnesium alloy negatively shifts from −1.319 V to −1.455 V and its corrosion rate increases, which indicates the increase of temperature significantly accelerates its anode process due to the damage of the structure of corrosion product film caused by hydrogen evolution. Moreover, the higher the temperature is, the more serious the damage of corrosion product film is.

2. It is surprising that, with the increase of immersion time, the activation energy of the corrosion reaction of AZ91D magnesium alloy decreases and the corrosion rate of AZ91D magnesium alloy increases, which may be attributed to the damage of the structure of corrosion product film by hydrogen evolution.

3. It is interesting that, in distilled water, the EIS of AZ91D magnesium alloy includes three time constants, and there is no inductive arc in the low frequency region.

4. The corrosion product film of AZ91D magnesium alloy in distilled water is composed of a compact inner corrosion product film and a relatively loose outer corrosion product film.

Acknowledgements

The authors thank the financial support of the National Natural Science Foundation of China (No. 51401151) and the Natural Science Foundation of Hubei (No. 2018CFB525).

References

Abdulov, R.Z., Valiev, R.Z., Krasilnikov, N.A., 1990. Formation of submicrometre-grained structure in magnesium alloy due to high plastic strains. J. Mater. Sci. Lett. 9, 1445–1447. https://doi.org/10.1007/bf00721611.

Aljinović, L.J., Gudić, S., Šmith, M., 2000. Inhibition of CuNi10Fe corrosion in seawater by sodium-diethyl-dithiocarbamate: an electrochemical and analytical study. J. Appl. Electrochem. 30, 973–979. https://doi.org/10.1023/A:1004074405514.

Arrabal, R., Pardo, A., Merino, M.C., Mohedano, M., Casajús, P., Paucarb, K., Garcés, G., 2012. Effect of Nd on the corrosion behaviour of AM50 and AZ91D magnesium alloys in 3.5 wt.% NaCl solution. Corros. Sci. 55, 301–312. https://doi.org/10.1016/j.electacta.2009.06.025.

Arrabal, R., Pardo, A., Merino, M.C., Mohedano, M., Casajús, P., Paucar, K., Garcés, G., 2012. Effect of Nd on the corrosion behaviour of AM50 and AZ91D magnesium alloys in 3.5 wt.% NaCl solution. Corros. Sci. 55, 301–312. https://doi.org/10.1016/j.corsci.2011.10.033.

Atrens, A., Song, G.L., Liu, M., Shi, Z., Cao, F., Dargusch, M.S., 2015. Review of recent developments in the field of magnesium corrosion. Adv. Eng. Mater. 17, 400–453. https://doi.org/10.1002/adem.201400434.

Atrens, A., Johnston, S., Shi, Z., Dargusch, M.S., 2018. Viewpoint-Understanding Mg corrosion in the body for biodegradable medical implants. Scripta Mater. 154, 92–100. https://doi.org/10.1016/j.scriptamat.2018.05.021.

Chen, J., Lin, W., Liang, S., Zou, L., Wang, C., Wang, B., Yan, M., Cui, X., 2019. Effect of alloy cations on corrosion resistance of LDH/MAO coating on magnesium alloy. Appl. Surf. Sci. 463, 535–544. https://doi.org/10.1016/j.apsusc.2018.08.242.

Coy, A.E., Viejo, F., Skeldon, P., Thompson, G.E., 2010. Susceptibility of rare-earth-magnesium alloys to micro-galvanic corrosion. Corros. Sci. 52, 3896–3906. https://doi.org/10.1016/j.corsci.2010.08.006.

Cui, Z., Li, X., Xiao, K., Dong, C., 2013. Atmospheric corrosion of field-exposed AZ31 magnesium in a tropical marine environment. Corros. Sci. 76, 243–256. https://doi.org/10.1016/j.corsci.2013.06.047.

Du, C.P., Xu, D.F., 2013. Application of Energy-Saving Magnesium Alloy in Automotive Industry. Adv. Mater. Res. 734–737, 2244–2247. https://doi.org/10.4028/www.scientific.net/AMR.734-737.2244.

Fekry, A.M., El-Sherif, R.M., 2009. Electrochemical corrosion behavior of magnesium and titanium alloys in simulated body fluid. Electrochim. Acta. 54, 7280–7285. https://doi.org/10.1016/j.electacta.2009.07.047.

Grosselle, F., Timelli, G., Bonollo, F., 2010. Doe applied to microstructural and mechanical properties of Al-Si-Cu-Mg casting alloys for automotive applications. Mat. Sci. Eng. A 527, 3536–3545. https://doi.org/10.1016/j.msea.2010.02.029.

Hänzi, A.C., Dalla, Torre F.H., Sologubenko, A.S., Gunde, P., Schmid-Fetzer, R., Kuehlein, M., Löffler, J.F., Uggowitzer, P.J., 2009. Design strategy for microalloyed ultra-ductile magnesium alloys. Phil. Mag. Lett. 89, 377–390. https://doi.org/10.1080/09500830902960125.

Huang, D., Hu, J., Song, G.L., Guo, X., 2012. Galvanic Corrosion and Inhibition of GW103 and AZ91D Mg Alloys Coupled to an Al Alloy in an Ethylene Glycol Solution at Ambient and Elevated Temperatures. Corros. 68, 475–488. https://doi.org/10.5006/i0010-9312-68-6-475.

Jiang, D.M., Kang, S.B., Kim, H.W., 1999. Microstructure and mechanical properties of Al-Mg alloy sheets for autobody application. Met. Sci. J. 15, 1401–1407. https://doi.org/10.1179/026708399101505536.

Jönsson, M., Dan, P., Thierry, D., 2007. Corrosion product formation during NaCl induced atmospheric corrosion of magnesium alloy AZ91D. Corros. Sci. 49, 1540–1558. https://doi.org/10.1016/j.corsci.2006.08.004.

Kwon, Y.J., Shigematsu, I., Saito, N., 2006. Dissimilar friction stir welding between magnesium and aluminum alloys. Mater. Lett. 62, 3827–3829. https://doi.org/10.1016/j.matlet.2008.04.080.

Li, Q., Li, X., Zhang, Q., Chen, J., 2010. Effect of rare-earth element Sm on the corrosion behavior of Mg6Al1.2Y-0.9Nd alloy. Rare Metals. 29, 557–560. https://doi.org/10.1007/s12598-010-0168-2.

Liao, J., Hotta, M., 2015. Atmospheric corrosion behavior of field-exposed magnesium alloys: Influences of chemical composition and microstructure. Corros. Sci. 100, 353–364. https://doi.org/10.1016/j.corsci.2015.08.021.

Lu, X., Feng, X., Zuo, Y., Zheng, C., Lu, S., Xu, L., 2015. Evaluation of the micro-arc oxidation treatment effect on the protective performance of a Mg-rich epoxy coating on AZ91D magnesium alloy. Surf. Coat. Tech. 270, 227–235. https://doi.org/10.1016/j.surfcoat.2015.02.052.

Medhashree, H., Shetty, A.N., 2017. Electrochemical investigation on the effects of sulfate ion concentration, temperature and medium pH on the corrosion behavior of Mg–Al–Zn–Mn alloy in aqueous ethylene glycol. J. Magnes. Alloy. 5, 64–73. https://doi.org/10.1016/j.jma.2016.12.003.

Mehta, S.D., Masood, S.H., Song, W.Q., 2004. Investigation of wear properties of magnesium and aluminum alloys for automotive applications. J. Mater. Process. Tech. 155, 1526–1531. https://doi.org/10.1016/j.jmatprotec.2004.04.247.

Nan, L., Zheng, Y., 2013. Novel Magnesium Alloys Developed for Biomedical Application: A Review. J. Mater. Sci. Technol. 29, 489–502. https://doi.org/10.1016/j.jmst.2013.02.005.

Phani, A.R., Gammel, F.J., Hack, T., Haefke, H., 2015. Enhanced corrosioon resistance by sol-gel-based ZrO_2-CeO_2 coatings on magnesium alloys. Mater. Corros. 56, 77–82. https://doi.org/10.1002/maco.200403823.

Qi, Z., Cong, B., Qi, B., Sun, H., Zhao, G., Ding, J., 2018. Microstructure and mechanical properties of double-wire plus arc additively manufactured Al-Cu-Mg alloys. J. Mater. Process. Tech. 255, 347–353. https://doi.org/10.1016/j.jmatprotec.2017.12.019.

Qu, Q., Li, S., Li, L., Zuo, L., Ran, X., Qu, Y., Zhu, B., 2017. Adsorption and corrosion behaviour of Trichoderma harzianum for AZ31B magnesium alloy in artificial seawater. Corros. Sci. 118, 12–23. https://doi.org/10.1016/j.corsci.2017.01.005.

Raj, X.J., Rajendran, N., 2013. Inhibition effect of newly synthesised piperidine derivatives on the corrosion of brass in natural seawater. Prot. Met. Phys. Chem. Surf. 49, 763–775. https://doi.org/10.1134/S2070205113060257.

Seetharaman, R., Lavanya, B., Niharika, N., Thyagarajan, P., 2017. Development and Performance Validation of Engine oil Pump for Passenger Cars Using Magnesium Alloy. Mater. Today: Proceedings. 4, 6743–6749. https://doi.org/10.1016/j.matpr.2017.06.450.

Shi, C., Li, H., Wang, D., Zuo, T., Li, Y., 2001. A proposal on accelerating development of metallic magnesium industry in china. Mater. Rev. 15, 5–6 http://en.cnki.com.cn/Article_en/CJFDTotal-CLDB200104002.htm.

Shi, Z., Liu, M., Atrens, A., 2010. Measurement of the corrosion rate of magnesium alloys using Tafel extrapolation. Corros. Sci. 52, 579–588. https://doi.org/10.1016/j.corsci.2009.10.016.

Song, G., Atrens, A., Stjohn, D., Nairn, J., Li, Y., 1997. The electrochemical corrosion of pure magnesium in 1 N NaCl. Corros. Sci. 39 (5), 855–875. https://doi.org/10.1016/S0010-938X(96)00172-2.

Song, G., Atrens, A., 1999. Corrosion mechanisms of magnesium alloys. Adv. Eng. Mater. 1, 11–33. https://doi.org/10.1002/(SICI)1527-2648(199909)1:1<11::AID-ADEM11>3.0.CO;2-N.

Song, G., Atrens, A., 2003. Understanding magnesium corrosion mechanism: a framework for improved alloy performance. Adv. Eng. Mater. 5, 837–858. https://doi.org/10.1002/adem.200310405.

Song, G., Johannesson, B., Hapugoda, S., Stjohn, D., 2004. Galvanic corrosion of magnesium alloy AZ91D in contact with an alu-

minium alloy, steel and zinc. Corros. Sci. 46, 955–977. https://doi.org/10.1016/S0010-938X(03)00190-2.

Song, Y.W., Shan, D.Y., Han, E.H., 2008. Electrodeposition of hydroxyapatite coating on AZ91D magnesium alloy for biomaterial application. Mater. Let. 62, 3276–3279. https://doi.org/10.1016/j.matlet.2008.02.048.

Staiger, M.P., Pietak, A.M., Huadmai, J., Dias, G., 2006. Magnesium and its alloys as orthopedic biomaterials: a review. Biomaterials. 27, 1728–1734. https://doi.org/10.1016/j.biomaterials.2005.10.003.

Wang, H., Akid, R., Gobara, M., 2010. Scratch-resistant anticorrosion sol–gel coating for the protection of AZ31 magnesium alloy via a low temperature sol–gel route. Corros. Sci. 52, 2565–2570. https://doi.org/10.1016/j.corsci.2010.04.002.

Yang, L., Huang, Y., Feyerabend, F., Willumeit, R., Mendis, C., Kainer, K.U., Hort, N., 2013. Microstructure, mechanical and corrosion properties of Mg-Dy-Gd-Zr alloys for medical applications. Acta Biomater. 9, 8499–8508. https://doi.org/10.1016/j.actbio.2013.03.017.

Zhang, J., Gu, C., Tong, Y., Yan, W., Tu, J., 2016. A Smart Superhydrophobic Coating on AZ31B Magnesium Alloy with Self-Healing Effect. Adv. Mater. Interfaces. 3, 1500694. https://doi.org/10.1002/admi.201500694.

Zhang, Q.H., Hou, B.S., Xu, N., Liu, H.F., Zhang, G.A., 2019. Two novel thiadiazole derivatives as highly efficient inhibitors for the corrosion of mild steel in the CO_2-saturated oilfield produced water. J. Taiwan Inst. Chem. E. 96, 588–598. https://doi.org/10.1016/j.jtice.2018.11.022.

Zhang, Y., Shao, Y., Zhang, T., Meng, G., Wang, F., 2011. The effect of epoxy coating containing emeraldine base and hydrofluoric acid doped polyaniline on the corrosion protection of AZ91D magnesium alloy. Corros. Sci. 53, 3747–3755. https://doi.org/10.1016/j.corsci.2011.07.021.

Zhang, P., Zuo, Y., 2019. Relationship between porosity, pore parameters and properties of microarc oxidation film on AZ91D magnesium alloy. Results Phys. 12, 2044–2054. https://doi.org/10.1016/j.rinp.2019.01.095.